A Deslauriers-Dubuc interpolation function ϕ has the shortest support while including polynomials of degree $2p-1$ in the spaces $\mathbf{V}_j$. The corresponding interpolation filter $h_i[n]$ defined by (7.214) has $2p$ non-zero coefficients for $-p \leqslant n < p$, which are calculated in (7.201). If $p=2$ then $h_i[1] = h_i[-2] = -1/16$ and $h_i[0] = h_i[-1] = 9/16$. Suppose that $q(t)$ is a polynomial of degree smaller or equal to $2p-1$. Since $q = P_{\mathbf{V}_j} q$, (7.213) implies a Lagrange interpolation formula

$$q\Big(2^j\,(n+1/2)\Big) = \sum_{k=-\infty}^{+\infty} q(2^j k)\, h_i[n-k]\ .$$

The Lagrange filter h_i of size $2p$ is the shortest filter that recovers intermediate values of polynomials of degree $2p-1$ from a uniform sampling.

To restrict the wavelet interpolation bases to a finite interval $[0,1]$ while reproducing polynomials of degree $2p-1$, the filter h_i is modified at the boundaries. Suppose that $f(N^{-1}n)$ is defined for $0 \leqslant n < N$. When computing the interpolation

$$P_{\mathbf{V}_j} f\Big(2^j\,(n+1/2)\Big) = \sum_{k=-\infty}^{+\infty} f(2^j k)\, h_i[n-k],$$

if n is too close to 0 or to $2^{-j}-1$ then h_i must be modified to ensure that the support of $h_i[n-k]$ remains inside $[0, 2^{-j}-1]$. The interpolation $P_{\mathbf{V}_j} f(2^j(n+1/2))$ is then calculated from the closest $2p$ samples $f(2^j k)$ for $2^j k \in [0,1]$. The new interpolation coefficients are computed in order to recover exactly all polynomials of degree $2p-1$ [450]. For $p=2$, the problem occurs only at $n=0$ and the appropriate boundary coefficients are

$$h_i[0] = \frac{5}{16}\ ,\ h_i[-1] = \frac{15}{16}\ ,\ h_i[-2] = \frac{-5}{16}\ ,\ h_i[-3] = \frac{1}{16}\ .$$

The symmetric boundary filter $h_i[-n]$ is used on the other side at $n = 2^{-j}-1$.

7.7 Separable Wavelet Bases

To any wavelet orthonormal basis $\{\psi_{j,n}\}_{(j,n)\in\mathbb{Z}^2}$ of $\mathbf{L^2}(\mathbb{R})$, one can associate a separable wavelet orthonormal basis of $\mathbf{L^2}(\mathbb{R}^2)$:

$$\Big\{\psi_{j_1,n_1}(x_1)\,\psi_{j_2,n_2}(x_2)\Big\}_{(j_1,j_2,n_1,n_2)\in\mathbb{Z}^4}\ . \tag{7.215}$$

The functions $\psi_{j_1,n_1}(x_1)\,\psi_{j_2,n_2}(x_2)$ mix information at two different scales 2^{j_1} and 2^{j_2} along x_1 and x_2, which we often want to avoid. Separable multiresolutions lead to another construction of separable wavelet bases whose elements are products of functions dilated at the same scale. These multiresolution approximations also have important applications in computer vision, where they are used to process images at different levels of details. Lower resolution images are indeed represented by fewer pixels and might still carry enough information to perform a recognition task.

Signal decompositions in separable wavelet bases are computed with a separable extension of the filter bank algorithm described in Section 7.7.3. Section 7.7.4 constructs separable wavelet bases in any dimension, and explains the corresponding fast wavelet transform algorithm. Non-separable wavelet bases can also be constructed [83, 333] but they are used less often in image processing. Section 7.8.3 gives examples of non-separable quincunx biorthogonal wavelet bases, which have a single quasi-istropic wavelet at each scale.

7.7.1 Separable Multiresolutions

As in one dimension, the notion of resolution is formalized with orthogonal projections in spaces of various sizes. The approximation of an image $f(x_1,x_2)$ at the resolution 2^{-j} is defined as the orthogonal projection of f on a space $\mathbf{V}_j^2$ that is included in $\mathbf{L^2}(\mathbb{R}^2)$. The space $\mathbf{V}_j^2$ is the set of all approximations at the resolution 2^{-j}. When the resolution decreases, the size of $\mathbf{V}_j^2$

decreases as well. The formal definition of a multiresolution approximation $\{\mathbf{V}_j^2\}_{j\in\mathbb{Z}}$ of $\mathbf{L^2}(\mathbb{R}^2)$ is a straightforward extension of Definition 7.1 that specifies multiresolutions of $\mathbf{L^2}(\mathbb{R})$. The same causality, completeness and scaling properties must be satisfied.

We consider the particular case of separable multiresolutions. Let $\{\mathbf{V}_j\}_{j\in\mathbb{Z}}$ be a multiresolution of $\mathbf{L^2}(\mathbb{R})$. A separable two-dimensional multiresolution is composed of the tensor product spaces

$$\mathbf{V}_j^2 = \mathbf{V}_j \otimes \mathbf{V}_j \ . \tag{7.216}$$

The space $\mathbf{V}_j^2$ is the set of finite energy functions $f(x_1, x_2)$ that are linear expansions of separable functions:

$$f(x_1,x_2) = \sum_{m=-\infty}^{+\infty} a[m]\, f_m(x_1)\, g_m(x_2) \quad \text{with} \quad f_m \in \mathbf{V}_j \ , \ g_m \in \mathbf{V}_j \ .$$

Section A.5 reviews the properties of tensor products. If $\{\mathbf{V}_j\}_{j\in\mathbb{Z}}$ is a multiresolution approximation of $\mathbf{L^2}(\mathbb{R})$ then $\{\mathbf{V}_j^2\}_{j\in\mathbb{Z}}$ is a multiresolution approximation of $\mathbf{L^2}(\mathbb{R}^2)$.

Theorem 7.1 demonstrates the existence of a scaling function ϕ such that $\{\phi_{j,m}\}_{m\in\mathbb{Z}}$ is an orthonormal basis of $\mathbf{V}_j$. Since $\mathbf{V}_j^2 = \mathbf{V}_j \otimes \mathbf{V}_j$, Theorem A.6 proves that for $x = (x_1, x_2)$ and $n = (n_1, n_2)$

$$\left\{ \phi^2_{j,n}(x) = \phi_{j,n_1}(x_1)\, \phi_{j,n_2}(x_2) = \frac{1}{2^j}\, \phi\Big(\frac{x_1 - 2^j n_1}{2^j}\Big)\, \phi\Big(\frac{x_2 - 2^j n_2}{2^j}\Big) \right\}_{n\in\mathbb{Z}^2}$$

is an orthonormal basis of $\mathbf{V}_j^2$. It is obtained by scaling by 2^j the two-dimensional separable scaling function $\phi^2(x) = \phi(x_1)\,\phi(x_2)$ and translating it on a two-dimensional square grid with intervals 2^j.

Example 7.13. Piecewise constant approximation *Let $\mathbf{V}_j$ be the approximation space of functions that are constant on $[2^j m, 2^j(m+1)]$ for any $m \in \mathbb{Z}$. The tensor product defines a two-dimensional piecewise constant approximation. The space $\mathbf{V}_j^2$ is the set of functions that are constant on any square $[2^j n_1, 2^j(n_1+1)] \times [2^j n_2, 2^j(n_2+1)]$, for $(n_1, n_2) \in \mathbb{Z}^2$. The two dimensional scaling function is*

$$\phi^2(x) = \phi(x_1)\,\phi(x_2) = \begin{cases} 1 & \text{if } 0 \leqslant x_1 \leqslant 1 \text{ and } 0 \leqslant x_2 \leqslant 1 \\ 0 & \text{otherwise} \end{cases} .$$

Example 7.14. Shannon approximation *Let $\mathbf{V}_j$ be the space of functions whose Fourier transforms have a support included in $[-2^{-j}\pi, 2^{-j}\pi]$. The space $\mathbf{V}_j^2$ is the set of functions whose two-dimensional Fourier transforms have a support included in the low-frequency square $[-2^{-j}\pi, 2^{-j}\pi] \times [-2^{-j}\pi, 2^{-j}\pi]$. The two-dimensional scaling function is a perfect two-dimensional low-pass filter whose Fourier transform is*

$$\hat\phi(\omega_1)\,\hat\phi(\omega_2) = \begin{cases} 1 & \text{if } |\omega_1| \leqslant 2^{-j}\pi \text{ and } |\omega_2| \leqslant 2^{-j}\pi \\ 0 & \text{otherwise} \end{cases} .$$

Example 7.15. Spline approximation *Let $\mathbf{V}_j$ be the space of polynomial spline functions of degree p that are $\mathbf{C}^{p-1}$, with nodes located at $2^{-j}m$ for $m \in \mathbb{Z}$. The space $\mathbf{V}_j^2$ is composed of two-dimensional polynomial spline functions that are $p-1$ times continuously differentiable. The restriction of $f(x_1, x_2) \in \mathbf{V}_j^2$ to any square $[2^j n_1, 2^j(n_1+1)) \times [2^j n_2, 2^j(n_2+1))$ is a separable product $q_1(x_1)q_2(x_2)$ of two polynomials of degree at most p.*

Multiresolution Vision An image of 512 by 512 pixels often includes too much information for real time vision processing. Multiresolution algorithms process less image data by selecting the relevant details that are necessary to perform a particular recognition task [57]. The human visual system uses a similar strategy. The distribution of photoreceptors on the retina is not uniform. The visual acuity is greatest at the center of the retina where the density of receptors is maximum. When moving apart from the center, the resolution decreases proportionally to the distance from the retina center [427].

The high resolution visual center is called the *fovea*. It is responsible for high acuity tasks such as reading or recognition. A retina with a uniform resolution equal to the highest fovea resolution

Figure 7.21: Multiresolution approximations $a_j[n_1, n_2]$ of an image at scales 2^j, for $-5 \geqslant j \geqslant -8$.

would require about 10,000 times more photoreceptors. Such a uniform resolution retina would increase considerably the size of the optic nerve that transmits the retina information to the visual cortex and the size of the visual cortex that processes this data.

Active vision strategies [81] compensate the non-uniformity of visual resolution with eye saccades, which move successively the fovea over regions of a scene with a high information content. These saccades are partly guided by the lower resolution information gathered at the periphery of the retina. This multiresolution sensor has the advantage of providing high resolution information at selected locations, and a large field of view, with relatively little data.

Multiresolution algorithms implement in software [124] the search for important high resolution data. A uniform high resolution image is measured by a camera but only a small part of this information is processed. Figure 7.21 displays a pyramid of progressively lower resolution images calculated with a filter bank presented in Section 7.7.3. Coarse to fine algorithms analyze first the lower resolution image and selectively increase the resolution in regions where more details are needed. Such algorithms have been developed for object recognition, and stereo calculations [283].

7.7.2 Two-Dimensional Wavelet Bases

A separable wavelet orthonormal basis of $\mathbf{L^2}(\mathbb{R}^2)$ is constructed with separable products of a scaling function ϕ and a wavelet ψ. The scaling function ϕ is associated to a one-dimensional multiresolution approximation $\{\mathbf{V}_j\}_{j\in\mathbb{Z}}$. Let $\{\mathbf{V}_j^2\}_{j\in\mathbb{Z}}$ be the separable two-dimensional multiresolution defined by $\mathbf{V}_j^2 = \mathbf{V}_j \otimes \mathbf{V}_j$. Let $\mathbf{W}_j^2$ be the detail space equal to the orthogonal complement of the lower resolution approximation space $\mathbf{V}_j^2$ in $\mathbf{V}_{j-1}^2$:

$$\mathbf{V}_{j-1}^2 = \mathbf{V}_j^2 \oplus \mathbf{W}_j^2 \ . \tag{7.217}$$

To construct a wavelet orthonormal basis of $\mathbf{L^2}(\mathbb{R}^2)$, the following theorem builds a wavelet basis of each detail space $\mathbf{W}_j^2$.

Theorem 7.25. *Let ϕ be a scaling function and ψ be the corresponding wavelet generating a wavelet orthonormal basis of $\mathbf{L^2}(\mathbb{R})$. We define three wavelets:*

$$\psi^1(x) = \phi(x_1)\,\psi(x_2) \quad , \quad \psi^2(x) = \psi(x_1)\,\phi(x_2) \quad , \quad \psi^3(x) = \psi(x_1)\,\psi(x_2), \tag{7.218}$$

and denote for $1 \leqslant k \leqslant 3$

$$\psi_{j,n}^k(x) = \frac{1}{2^j}\,\psi^k\left(\frac{x_1 - 2^j n_1}{2^j}, \frac{x_2 - 2^j n_2}{2^j}\right).$$

The wavelet family

$$\left\{\psi_{j,n}^1 \ , \ \psi_{j,n}^2 \ , \ \psi_{j,n}^3\right\}_{n\in\mathbb{Z}^2} \tag{7.219}$$

is an orthonormal basis of $\mathbf{W}_j^2$ and

$$\left\{\psi_{j,n}^1 \ , \ \psi_{j,n}^2 \ , \ \psi_{j,n}^3\right\}_{(j,n)\in\mathbb{Z}^3} \tag{7.220}$$

is an orthonormal basis of $\mathbf{L^2}(\mathbb{R}^2)$.

Proof. Equation (7.217) is rewritten

$$\mathbf{V}_{j-1} \otimes \mathbf{V}_{j-1} = (\mathbf{V}_j \otimes \mathbf{V}_j) \oplus \mathbf{W}_j^2 \ . \tag{7.221}$$

The one-dimensional multiresolution space $\mathbf{V}_{j-1}$ can also be decomposed into $\mathbf{V}_{j-1} = \mathbf{V}_j \oplus \mathbf{W}_j$. By inserting this in (7.221), the distributivity of $\oplus$ with respect to $\otimes$ proves that

$$\mathbf{W}_j^2 = (\mathbf{V}_j \otimes \mathbf{W}_j) \oplus (\mathbf{W}_j \otimes \mathbf{V}_j) \oplus (\mathbf{W}_j \otimes \mathbf{W}_j) \ . \tag{7.222}$$

Since $\{\phi_{j,m}\}_{m\in\mathbb{Z}}$ and $\{\psi_{j,m}\}_{m\in\mathbb{Z}}$ are orthonormal bases of $\mathbf{V}_j$ and $\mathbf{W}_j$, we derive that

$$\{\phi_{j,n_1}(x_1)\,\psi_{j,n_2}(x_2)\ ,\ \psi_{j,n_1}(x_1)\,\phi_{j,n_2}(x_2)\ ,\ \psi_{j,n_1}(x_1)\,\psi_{j,n_2}(x_2)\}_{(n_1,n_2)\in\mathbb{Z}^2}$$

is an orthonormal basis of $\mathbf{W}_j^2$. As in the one-dimensional case, the overall space $\mathbf{L^2}(\mathbb{R}^2)$ can be decomposed as an orthogonal sum of the detail spaces at all resolutions:

$$\mathbf{L^2}(\mathbb{R}^2) = \oplus_{j=-\infty}^{+\infty} \mathbf{W}_j^2. \tag{7.223}$$

Hence

$$\{\phi_{j,n_1}(x_1)\,\psi_{j,n_2}(x_2)\ ,\ \psi_{j,n_1}(x_1)\,\phi_{j,n_2}(x_2)\ ,\ \psi_{j,n_1}(x_1)\,\psi_{j,n_2}(x_2)\}_{(j,n_1,n_2)\in\mathbb{Z}^3}$$

is an orthonormal basis of $\mathbf{L^2}(\mathbb{R}^2)$. ■ ■

The three wavelets extract image details at different scales and in different directions. Over positive frequencies, $\hat{\phi}$ and $\hat{\psi}$ have an energy mainly concentrated respectively on $[0,\pi]$ and $[\pi,2\pi]$. The separable wavelet expressions (7.218) imply that

$$\hat{\psi}^1(\omega_1,\omega_2) = \hat{\phi}(\omega_1)\,\hat{\psi}(\omega_2)\ ,\ \hat{\psi}^2(\omega_1,\omega_2) = \hat{\psi}(\omega_1)\,\hat{\phi}(\omega_2)$$

and $\hat{\psi}^3(\omega_1,\omega_2) = \hat{\psi}(\omega_1)\,\hat{\psi}(\omega_2)$. Hence $|\hat{\psi}^1(\omega_1,\omega_2)|$ is large at low horizontal frequencies ω_1 and high vertical frequencies ω_2, whereas $|\hat{\psi}^2(\omega_1,\omega_2)|$ is large at high horizontal frequencies and low vertical frequencies, and $|\hat{\psi}_3(\omega_1,\omega_2)|$ is large at at high horizontal and vertical frequencies. Figure 7.22 displays the Fourier transform of separable wavelets and scaling functions calculated from a one-dimensional Daubechies 4 wavelet.

Suppose that $\psi(t)$ has p vanishing moments and is thus orthogonal to one-dimensional polynomials of degree $p-1$. The wavelet ψ^1 has p one-dimensional directional vanishing moments along x_2 in the sense that it is orthogonal to any function $f(x_1,x_2)$ that is a polynomial of degree $p-1$ along x_2 for x_1 fixed. It is a horizontal directional wavelet that yields large coefficients for horizontal edges, as explained in Section 5.5.1. Similarly, ψ^2 has $p-1$ directional vanishing moments along x_1 and is a vertical directional wavelet. This is illustrated by the decomposition of a square in Figure 7.24. The wavelet ψ^3 has directional vanishing moments along both x_1 and x_2 and is therefore not a directional wavelet. It produces large coefficients at corners or junctions. The three wavelets ψ^k for $k=1,2,3$ are orthogonal to two-dimensional polynomials of degree $p-1$.

Example 7.16. *For a Shannon multiresolution approximation, the resulting two-dimensional wavelet basis paves the two-dimensional Fourier plane* (ω_1,ω_2) *with dilated rectangles. The Fourier transforms* $\hat{\phi}$ *and* $\hat{\psi}$ *are the indicator functions respectively of* $[-\pi,\pi]$ *and* $[-2\pi,-\pi]\cup[\pi,2\pi]$. *The separable space* $\mathbf{V}_j^2$ *contains functions whose two-dimensional Fourier transforms have a support included in the low-frequency square* $[-2^{-j}\pi,2^{-j}\pi]\times[-2^{-j}\pi,2^{-j}\pi]$. *This corresponds to the support of* $\hat{\phi}_{j,n}^2$ *indicated in Figure 7.23. The detail space* $\mathbf{W}_j^2$ *is the orthogonal complement of* $\mathbf{V}_j^2$ *in* $\mathbf{V}_{j-1}^2$ *and thus includes functions whose Fourier transforms have a support in the frequency annulus between the two squares* $[-2^{-j}\pi,2^{-j}\pi]\times[-2^{-j}\pi,2^{-j}\pi]$ *and* $[-2^{-j+1}\pi,2^{-j+1}\pi]\times[-2^{-j+1}\pi,2^{-j+1}\pi]$. *As shown in Figure 7.23, this annulus is decomposed in three separable frequency regions, which are the Fourier supports of* $\hat{\psi}_{j,n}^k$ *for* $1\leqslant k\leqslant 3$. *Dilating these supports at all scales* 2^j *yields an exact cover of the frequency plane* (ω_1,ω_2).

For general separable wavelet bases, Figure 7.23 gives only an indication of the domains where the energy of the different wavelets is concentrated. When the wavelets are constructed with a one-dimensional wavelet of compact support, the resulting Fourier transforms have side lobes that appear in Figure 7.22.

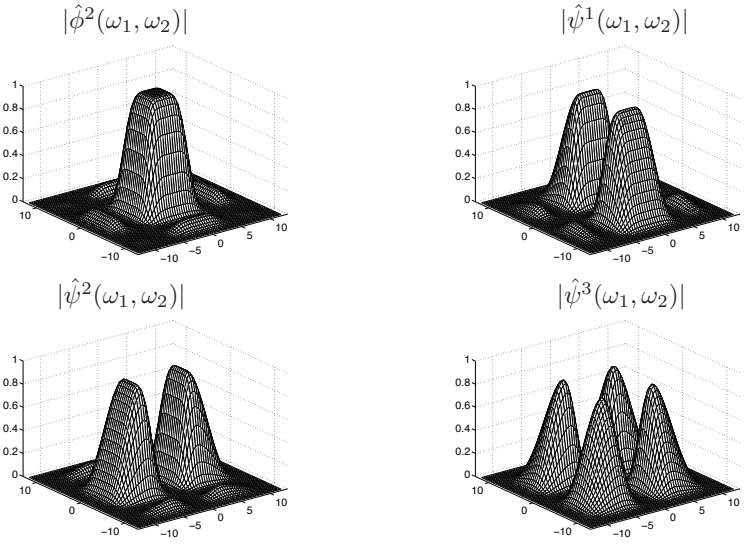

Figure 7.22: Fourier transforms of a separable scaling function and of 3 separable wavelets calculated from a one-dimensional Daubechies 4 wavelet.

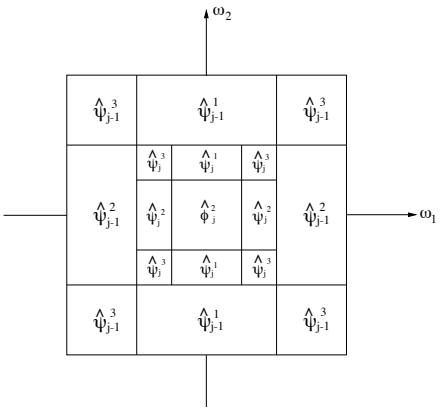

Figure 7.23: These dyadic rectangles indicate the regions where the energy of $\hat{\psi}^k_{j,n}$ is mostly concentrated, for $1 \leqslant k \leqslant 3$. Image approximations at the scale 2^j are restricted to the lower frequency square.

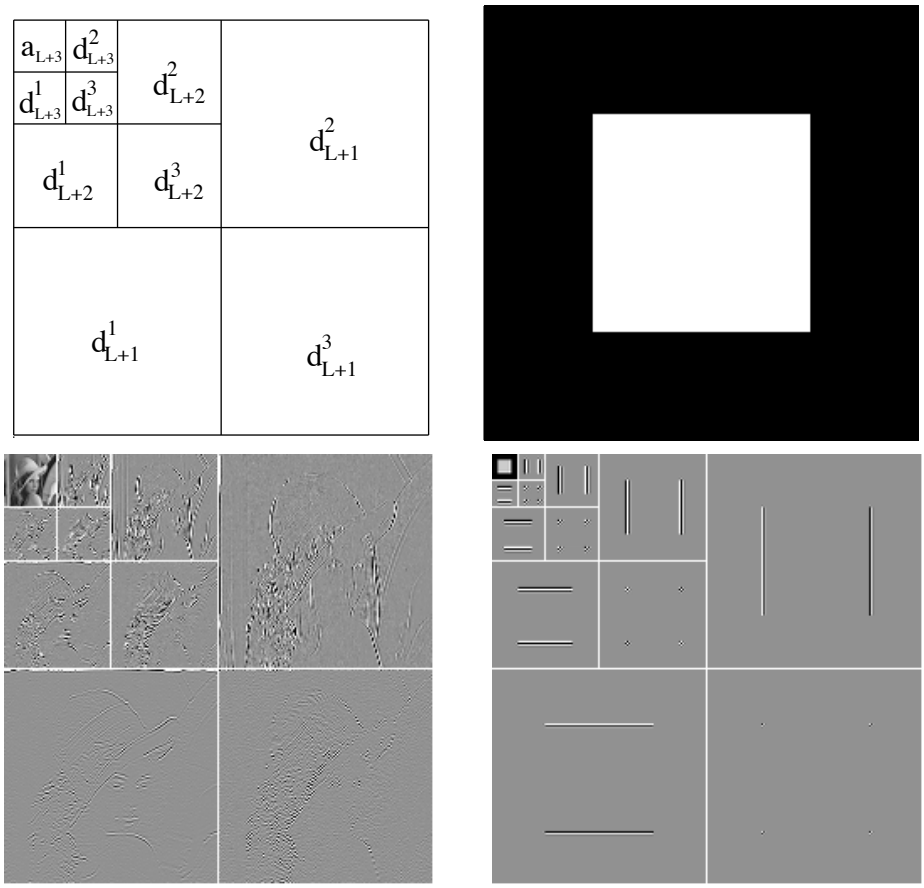

Figure 7.24: Separable wavelet transforms of Lena and of a white square in a black background, decomposed respectively on 3 and 4 octaves. Black, grey and white pixels correspond respectively to positive, zero and negative wavelet coefficients. The disposition of wavelet image coefficients $d_j^k[n,m] = \langle f, \psi_{j,n}^k \rangle$ is illustrated on the top left.

Example 7.17. *Figure 7.24 gives two examples of wavelet transforms computed using separable Daubechies wavelets with $p = 4$ vanishing moments. They are calculated with the filter bank algorithm of Section 7.7.3. Coefficients of large amplitude in d_j^1, d_j^2 and d_j^3 correspond respectively to vertical high frequencies (horizontal edges), horizontal high frequencies (vertical edges), and high frequencies in both directions (corners). Regions where the image intensity varies smoothly yield nearly zero coefficients, shown in grey. The large number of nearly zero coefficients makes it particularly attractive for compact image coding.*

Separable Biorthogonal Bases One-dimensional biorthogonal wavelet bases are extended to separable biorthogonal bases of $\mathbf{L^2}(\mathbb{R}^2)$ with the same approach as in Theorem 7.25. Let ϕ, ψ and $\tilde{\phi}$, $\tilde{\psi}$ be two dual pairs of scaling functions and wavelets that generate biorthogonal wavelet bases of $\mathbf{L^2}(\mathbb{R})$. The dual wavelets of ψ^1, ψ^2 and ψ^3 defined by (7.218) are

$$\tilde{\psi}^1(x) = \tilde{\phi}(x_1)\,\tilde{\psi}(x_2)\ ,\ \tilde{\psi}^2(x) = \tilde{\psi}(x_1)\,\tilde{\phi}(x_2)\ ,\ \tilde{\psi}^3(x) = \tilde{\psi}(x_1)\,\tilde{\psi}(x_2)\ . \tag{7.224}$$

One can verify that

$$\left\{\psi_{j,n}^1\ ,\ \psi_{j,n}^2\ ,\ \psi_{j,n}^3\right\}_{(j,n)\in\mathbb{Z}^3} \tag{7.225}$$

and

$$\left\{\tilde{\psi}_{j,n}^1\ ,\ \tilde{\psi}_{j,n}^2\ ,\ \tilde{\psi}_{j,n}^3\right\}_{(j,n)\in\mathbb{Z}^3} \tag{7.226}$$

are biorthogonal Riesz bases of $\mathbf{L^2}(\mathbb{R}^2)$.

7.7.3 Fast Two-Dimensional Wavelet Transform

The fast wavelet transform algorithm presented in Section 7.3.1 is extended in two dimensions. At all scales 2^j and for any $n = (n_1, n_2)$, we denote

$$a_j[n] = \langle f, \phi^2_{j,n} \rangle \quad \text{and} \quad d^k_j[n] = \langle f, \psi^k_{j,n} \rangle \quad \text{for } 1 \leqslant k \leqslant 3 \ .$$

For any pair of one-dimensional filters $y[m]$ and $z[m]$ we write the product filter $yz[n] = y[n_1]\, z[n_2]$, and $\bar{y}[m] = y[-m]$. Let $h[m]$ and $g[m]$ be the conjugate mirror filters associated to the wavelet ψ.

The wavelet coefficients at the scale 2^{j+1} are calculated from a_j with two-dimensional separable convolutions and subsamplings. The decomposition formula are obtained by applying the one-dimensional convolution formula (7.103) and (7.102) of Theorem 7.10 to the separable two-dimensional wavelets and scaling functions for $n = (n_1, n_2)$:

$$a_{j+1}[n] = a_j \star \bar{h}\bar{h}[2n] \ , \tag{7.227}$$
$$d^1_{j+1}[n] = a_j \star \bar{h}\bar{g}[2n] \ , \tag{7.228}$$
$$d^2_{j+1}[n] = a_j \star \bar{g}\bar{h}[2n] \ , \tag{7.229}$$
$$d^3_{j+1}[n] = a_j \star \bar{g}\bar{g}[2n] \ . \tag{7.230}$$

We showed in (3.70) that a separable two-dimensional convolution can be factored into one-dimensional convolutions along the rows and columns of the image. With the factorization illustrated in Figure 7.25(a), these four convolutions equations are computed with only six groups of one-dimensional convolutions. The rows of a_j are first convolved with $\bar{h}$ and $\bar{g}$ and subsampled by 2. The columns of these two output images are then convolved respectively with $\bar{h}$ and $\bar{g}$ and subsampled, which gives the four subsampled images a_{j+1}, d^1_{j+1}, d^2_{j+1} and d^3_{j+1}.

We denote by $\check{y}[n] = \check{y}[n_1, n_2]$ the image twice the size of $y[n]$, obtained by inserting a row of zeros and a column of zeros between pairs of consecutive rows and columns. The approximation a_j is recovered from the coarser scale approximation a_{j+1} and the wavelet coefficients d^k_{j+1} with two-dimensional separable convolutions derived from the one-dimensional reconstruction formula (7.104)

$$a_j[n] = \check{a}_{j+1} \star hh[n] + \check{d}^1_{j+1} \star hg[n] + \check{d}^2_{j+1} \star gh[n] + \check{d}^3_{j+1} \star gg[n] \ . \tag{7.231}$$

These four separable convolutions can also be factored into six groups of one-dimensional convolutions along rows and columns, illustrated in Figure 7.25(b).

Let $b[n]$ be an input image whose pixels have a distance 2^L. We associate to $b[n]$ a function $f(x) \in \mathbf{V}^2_L$ approximated at the scale 2^L. Its coefficients $a_L[n] = \langle f, \phi^2_{L,n} \rangle$ are defined like in (7.111) by

$$b[n] = 2^{-L}\, a_L[n] \approx f(2^L n) \ . \tag{7.232}$$

The wavelet image representation of a_L is computed by iterating (7.227-7.230) for $L \leqslant j < J$:

$$\left[a_J \ , \ \{d^1_j, d^2_j, d^3_j\}_{L < j \leqslant J} \right] \ . \tag{7.233}$$

The image a_L is recovered from this wavelet representation by computing (7.231) for $J > j \geqslant L$.

Finite Image and Complexity When a_L is a finite image of $N = N_1\, N_2$ pixels, we face boundary problems when computing the convolutions (7.227-7.231). Since the decomposition algorithm is separable along rows and columns, we use one of the three one-dimensional boundary techniques described in Section 7.5. The resulting values are decomposition coefficients in a wavelet basis of $\mathbf{L^2}[0,1]^2$. Depending on the boundary treatment, this wavelet basis is a periodic basis, a folded basis or a boundary adapted basis.

For square images with $N_1 = N_2$, the resulting images a_j and d^k_j have 2^{-2j} samples. The images of the wavelet representation (7.233) thus include a total of N samples. If h and g have size K, the reader can verify that $2K2^{-2(j-1)}$ multiplications and additions are needed to compute the four convolutions (7.227-7.230) with the factorization of Figure 7.25(a). The wavelet representation (7.233) is thus calculated with fewer than $8/3\ KN$ operations. The reconstruction of a_L by factoring the reconstruction equation (7.231) requires the same number of operations.

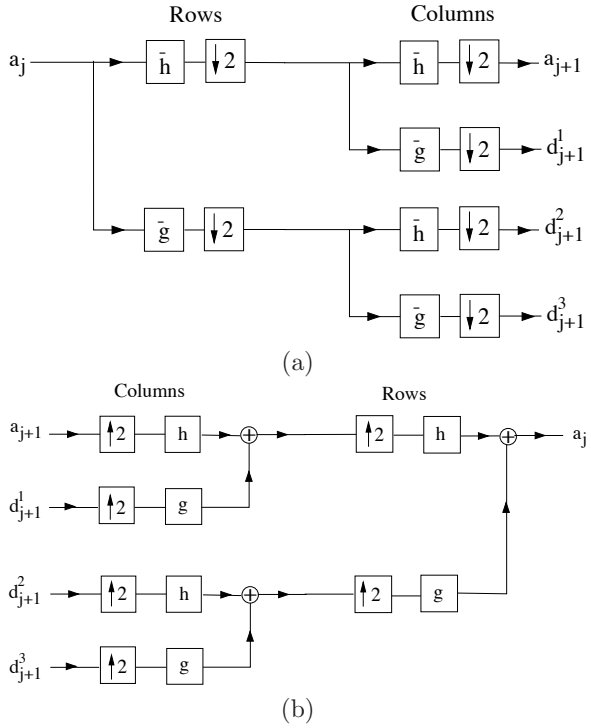

Figure 7.25: (a): Decomposition of a_j with 6 groups of one-dimensional convolutions and subsamplings along the image rows and columns. (b): Reconstruction of a_j by inserting zeros between the rows and columns of a_{j+1} and d^k_{j+1}, and filtering the output.

Fast Biorthogonal Wavelet Transform The decomposition of an image in a biorthogonal wavelet basis is performed with the same fast wavelet transform algorithm. Let $(\tilde{h}, \tilde{g})$ be the perfect reconstruction filters associated to (h, g). The inverse wavelet transform is computed by replacing the filters (h, g) that appear in (7.231) by $(\tilde{h}, \tilde{g})$.

7.7.4 Wavelet Bases in Higher Dimensions

Separable wavelet orthonormal bases of $\mathbf{L^2}(\mathbb{R}^p)$ are constructed for any $p \geqslant 2$, with a procedure similar to the two-dimensional extension. Let ϕ be a scaling function and ψ a wavelet that yields an orthogonal basis of $\mathbf{L^2}(\mathbb{R})$. We denote $\theta^0 = \phi$ and $\theta^1 = \psi$. To any integer $0 \leqslant \varepsilon < 2^p$ written in binary form $\varepsilon = \varepsilon_1 \dots, \varepsilon_p$ we associate the p-dimensional functions defined in $x = (x_1, \dots, x_p)$ by

$$\psi^{\varepsilon}(x) = \theta^{\varepsilon_1}(x_1) \dots \theta^{\varepsilon_n}(x_p)\,,$$

For $\varepsilon = 0$, we obtain a p-dimensional scaling function

$$\psi^0(x) = \phi(x_1) \dots \phi(x_p).$$

Non-zero indexes ε correspond to $2^p - 1$ wavelets. At any scale 2^j and for $n = (n_1, \dots, n_p)$ we denote

$$\psi^{\varepsilon}_{j,n}(x) = 2^{-pj/2}\, \psi^{\varepsilon}\Big(\frac{x_1 - 2^j n_1}{2^j}, \dots, \frac{x_p - 2^j n_p}{2^j}\Big)\,.$$

Theorem 7.26. *The family obtained by dilating and translating the $2^p - 1$ wavelets for $\varepsilon \neq 0$*

$$\Big\{\psi^{\varepsilon}_{j,n}\Big\}_{1 \leqslant \varepsilon < 2^p\,,\,(j,n) \in \mathbb{Z}^{p+1}} \tag{7.234}$$

is an orthonormal basis of $\mathbf{L^2}(\mathbb{R}^p)$.

The proof is done by induction on p. It follows the same steps as the proof of Theorem 7.25 which associates to a wavelet basis of $\mathbf{L^2}(\mathbb{R})$ a separable wavelet basis of $\mathbf{L^2}(\mathbb{R}^2)$. For $p = 2$, we verify that the basis (7.234) includes 3 elementary wavelets. For $p = 3$, there are 7 different wavelets.

Fast Wavelet Transform Let $b[n]$ be an input p-dimensional discrete signal sampled at intervals 2^L. We associate to $b[n]$ an approximation f at the scale 2^L whose scaling coefficients $a_L[n] = \langle f, \psi^0_{L,n} \rangle$ satisfy

$$b[n] = 2^{-Lp/2}\, a_L[n] \approx f(2^L n) \ .$$

The wavelet coefficients of f at scales $2^j > 2^L$ are computed with separable convolutions and subsamplings along the p signal dimensions. We denote

$$a_j[n] = \langle f, \psi^0_{j,n} \rangle \ \text{ and } \ d^\varepsilon_j[n] = \langle f, \psi^\varepsilon_{j,n} \rangle \ \text{ for } 0 < \varepsilon < 2^p \ .$$

The fast wavelet transform is computed with filters that are separable products of the one-dimensional filters h and g. The separable p-dimensional low-pass filter is

$$h^0[n] = h[n_1] \ldots h[n_p] \ .$$

Let us denote $u^0[m] = h[m]$ and $u^1[m] = g[m]$. To any integer $\varepsilon = \varepsilon_1 \ldots \varepsilon_p$ written in a binary form, we associate a separable p-dimensional band-pass filter

$$g^\varepsilon[n] = u^{\varepsilon_1}[n_1] \ldots u^{\varepsilon_p}[n_p].$$

Let $\bar{g}^\varepsilon[n] = g^\varepsilon[-n]$. One can verify that

$$a_{j+1}[n] = a_j \star \bar{h}^0[2n] \ , \tag{7.235}$$
$$d^\varepsilon_{j+1}[n] = a_j \star \bar{g}^\varepsilon[2n] \ . \tag{7.236}$$

We denote by $\check{y}[n]$ the signal obtained by adding a zero between any two samples of $y[n]$ that are adjacent in the p-dimensional lattice $n = (n_1, \ldots, n_p)$. It doubles the size of $y[n]$ along each direction. If $y[n]$ has M^p samples, then $\check{y}[n]$ has $(2M)^p$ samples. The reconstruction is performed with

$$a_j[n] = \check{a}_{j+1} \star h^0[n] + \sum_{\varepsilon=1}^{2^p-1} \check{d}^\varepsilon_{j+1} \star g^\varepsilon[n] \ . \tag{7.237}$$

The 2^p separable convolutions needed to compute a_j and $\{d^\varepsilon_j\}_{1 \leqslant \varepsilon \leqslant 2^p}$ as well as the reconstruction (7.237) can be factored in $2^{p+1} - 2$ groups of one-dimensional convolutions along the rows of p-dimensional signals. This is a generalization of the two-dimensional case, illustrated in Figures 7.25. The wavelet representation of a_L is

$$\left[\{d^\varepsilon_j\}_{1 \leqslant \varepsilon < 2^p \, , \, L < j \leqslant J} \ , \ a_J \right] \ . \tag{7.238}$$

It is computed by iterating (7.235) and (7.236) for $L \leqslant j < J$. The reconstruction of a_L is performed with the partial reconstruction (7.237) for $J > j \geqslant L$.

If a_L is a finite signal of size $N_1 \cdots N_p$, the one-dimensional convolutions are modified with one of the three boundary techniques described in Section 7.5. The resulting algorithm computes decomposition coefficients in a separable wavelet basis of $\mathbf{L^2}[0,1]^p$. If $N_1 = \cdots = N_p$, the signals a_j and d^ε_j have 2^{-pj} samples. Like a_L, the wavelet representation (7.238) is composed of N samples. If the filter h has K non-zero samples then the separable factorization of (7.235) and (7.236) requires $pK2^{-p(j-1)}$ multiplications and additions. The wavelet representation (7.238) is thus computed with fewer than $p(1 - 2^{-p})^{-1} KN$ multiplications and additions. The reconstruction is performed with the same number of operations.